ChemComm

COMMUNICATION

View Article Online
View Journal

Cite this: DOI: 10.1039/c6cc02544g

Received 24th March 2016,
Accepted 15th April 2016

DOI: 10.1039/c6cc02544g

www.rsc.org/chemcomm

Harnessing NMR relaxation interference effects to characterise supramolecular assemblies†

Gogulan Karunanithy,[a] Arjen Cnossen,[b] Henrik Müller,[a] Martin D. Peeks,[b] Nicholas H. Rees,[b] Timothy D. W. Claridge,[b] Harry L. Anderson[b] and Andrew J. Baldwin*[a]

Solution-state NMR spectroscopy remains the primary method for characterising synthetic supramolecular assemblies. Yet, in their NMR spectra, relaxation interference effects can significantly alter peak intensities hindering interpretation. Here, we present a simple experiment for synthetic chemists to analyse this effect, allowing interpretation of these distorted spectra and validation of spectral assignments. We apply this experiment to synthetic porphyrin oligomers with molecular weights approaching those of protein domains (10 kDa). Our experiment provides a simple means to gain additional structural and dynamical information that will become increasingly useful as chemists create larger molecular architectures.

Improvements in synthetic methodology have led to increasingly high molecular weight organic molecules. Illustrating this, methods have been developed for preparing covalent porphyrin oligomers with up to fifty porphyrin fragments[1] in cyclic[2,3] (Fig. 1A and Fig. S1, ESI†), linear[4] and tubular assemblies.[5] In solution-state NMR spectra of these complexes, puzzling anomalous patterns in homonuclear multiplet components have been observed, as exemplified by the β-pyrrole protons in a 10.2 kDa cyclic porphyrin hexamer (***c*-P6**, Fig. 1A). The effect resembles strong-coupling 'roofing', except that the relative intensities in one of the doublets is reversed (Fig. 1A), and the effect is present in the weak-coupling limit. Intriguingly, this effect becomes more pronounced as the molecular weight of the system increases (Fig. 1B), inviting us to take a thorough experimental and theoretical investigation into the origin of this behaviour.

In general, the relaxation rates of different components of a scalar coupled multiplet are not identical. Relaxation in NMR is caused by molecular motion producing rapidly fluctuating magnetic fields at the spin under study.[6,7] The main sources of these fields for spin-1/2 nuclei are dipolar interactions and chemical shift anisotropy (CSA), a measure of the angular dependence of shielding or de-shielding by proximate functional groups. In a rigid molecule, fluctuations in the two fields are correlated, which can lead them to interfere both constructively and destructively[8,9] for different parts of a scalar coupled multiplet (Fig. 2A). This 'relaxation interference' results in different components within a scalar coupled resonance showing different linewidths and intensities (Fig. 2A). To the best of our knowledge, these effects have not previously been directly observable in NMR spectra of synthetic molecular structures, although they

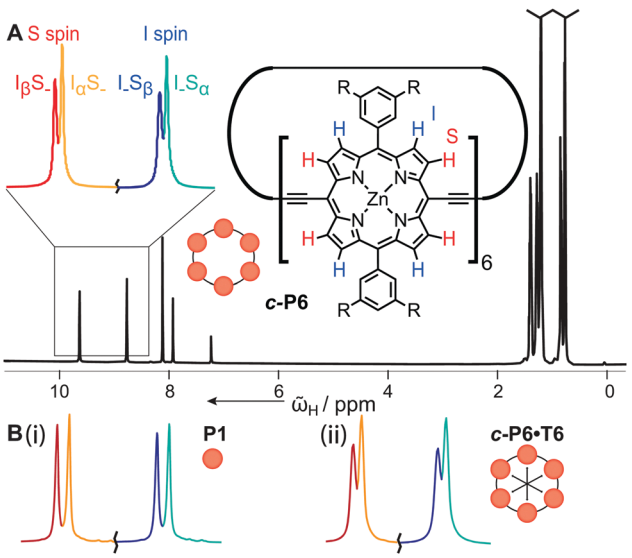

Fig. 1 (A) ^{1}H spectrum of a cyclic six porphyrin ring ***c*-P6** measured at 600 MHz together with its structure (inset, R = $Si(C_6H_{13})_3$) and schematic representation. The β-pyrrole proton adjacent to the aryl group is 'I' and that adjacent to the alkyne is 'S'. The porphyrins used in this study have one of three R groups: R = $Si(C_6H_{13})_3$ (THS), *t*-Bu or OC_8H_{17}. Here, the relatively broad component of each doublet is associated with the β state of the coupled spin ($J > 0$). (B) The ^{1}H resonances from the β-pyrrole protons of (i) **P1** (R = *t*-Bu) and (ii) ***c*-P6·T6** (R = THS). The anomalous effect is more prominent in the larger oligomer.

[a] *Department of Chemistry, University of Oxford, Physical and Theoretical Chemistry Laboratory, Oxford, OX1 3QZ, UK. E-mail: andrew.baldwin@chem.ox.ac.uk*

[b] *Department of Chemistry, University of Oxford, Chemistry Research Laboratory, Oxford, OX1 3TA, UK*

† Electronic supplementary information (ESI) available: Experimental and analysis details. See DOI: 10.1039/c6cc02544g

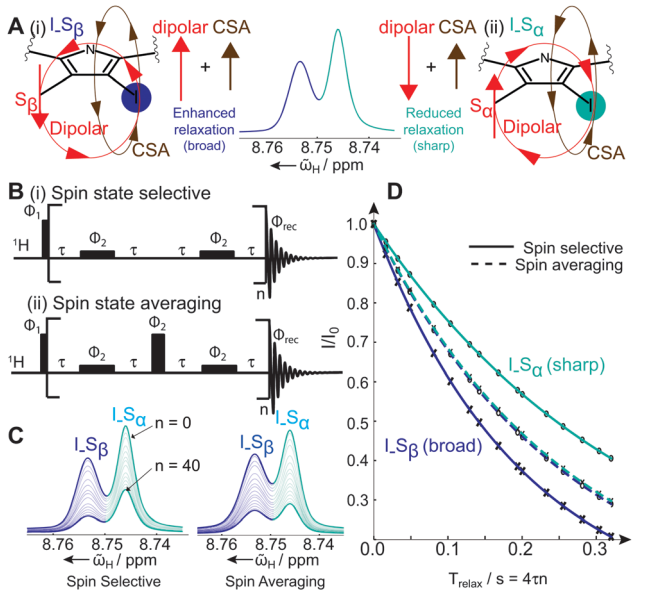

Fig. 2 (A) Magnetic fields induced by the dipolar and CSA interactions can interfere constructively (i) or destructively (ii) to give broader (i) or sharper (ii) resonances. (B(i)) Pulse sequence used to measure relaxation interference rate for individual components (ii) Inserting a high power 180° degree pulse mixes α and β spin states to give average relaxation rates. The tall black pulses are at maximum amplifier power and the shorter ones are low power 180° pulses of duration $(\sqrt{3}/2)\Delta\nu$ where $\Delta\nu$ is the difference in chemical shift $|\nu_I - \nu_S|$ in Hz and phase cycles $\Phi_1 = (x, y, -x, -y)$, $\Phi_2 = (y, -x, -y, x)$ and $\Phi_{rec} = (x, y, -x, -y)$. The total duration of relaxation period $T_{relax} = 4\tau n$ where τ = 2 ms. (C) The two pulse sequences give peaks with different ratios of heights. (D) Under sequence (B(i)) the two components of the I spin doublet relax at distinct rates whereas under sequence (B(ii)) they appear to relax at the same rate.

are frequently encountered in the field of biomolecular NMR. Moreover, techniques have been developed that exploit relaxation interference, selecting only the destructively interfering components. Such 'TROSY' spectra enable macromolecules up to the MDa range to be studied.[10–14] The intensity distribution and relaxation rates that define a scalar coupled multiplet contain detailed information about both the CSA, which depends on the electronic structure of the molecule, and the rate at which the molecule tumbles in solution. Although heteronuclear cross relaxation effects have been exploited in biomolecular studies, homonuclear effects have received relatively little attention. The move toward larger synthetic systems demands that these effects are properly recognised in chemical NMR applications and the potential for their exploitation realised. The methodology presented here addresses these needs directly, providing both a simple pulse sequences to reveal the effect (available in Bruker, Varian and GE Omega formats), and the computational means to analyse the data (Section S3, ESI†).

To reveal the effects of relaxation interference, it is necessary to measure relaxation rates of the individual components of a multiplet. In the case of a homonuclear doublet, the individual components can be associated with the coherence of the peak of interest (denoted '–') and the spin state of the coupled nucleus (denoted 'α' or 'β'). The four observed resonances from a homonuclear AX spin system are identified as I_-S_α, I_-S_β, $I_\alpha S_-$ and $I_\beta S_-$. Transverse relaxation rates would conventionally be measured using a CPMG[15,16] sequence or similar.[17] In such experiments α and β spin states of the coupled spin will be switched by each 180° pulse in the non-selective CPMG pulse train, averaging out any relaxation interference effects (Fig. 2D). Here, we put forward a simple homonuclear spin-state selective pulse sequence suitable for this task.

Decoupling each spin from its scalar coupled partner requires 'semi-selective' refocusing[18] where the chemical shift of the spin of interest (–) is inverted at intervals, and not the spin of the coupled nucleus ('α' or 'β'). To avoid the need for longer pulse durations which could challenge measurement of large R_2 values (Fig. S3, ESI†), we achieve spin state selective decoupling here through the use of selective low-power rectangular pulses.[19] If the duration of the pulse is set to $(\sqrt{3}/2)\Delta\nu$ where $\Delta\nu$ is frequency difference in Hz between the I and S spins, and the B_1 field calibrated such that the on-resonance spin is inverted, the coupled spin will experience no excitation (Fig. S3, ESI†). The pulse sequence (Fig. 2B) is run for a variable number of refocusing blocks, and the intensity of each peak, I, is recorded as a function of time, t, allowing the effective relaxation rate, R_2, to be determined from $I = I_0 e^{-R_2 t}$. Due to overlap between the individual components, it is necessary to fit the doublet shape as the sum of two resonances, subject to the restraints that peak position and shape do not vary with time (Section S3, ESI†). From this procedure, the rates $R_2^{I_-S_\beta}$ and $R_2^{I_-S_\alpha}$ are obtained with the 180° pulse zero excitation point set to the S spin chemical shift. The second doublet is measured by switching the S and I labels. While both rates appear identical using a conventional CPMG experiment, differences are revealed with our selective pulse sequence (Fig. 2C and D).

The relaxation rates of the multiplet components can be derived using the Redfield equation for an AX spin system[8,20] (and for AX_n more generally, Section S5, ESI†):

$$R_2^{I_-S_\alpha} = \left(R_D^2 + R_C^2 + 2P_2^0\cos(\theta)R_C R_D\right)f + R_D^2 f_{ADD}$$

$$R_2^{I_-S_\beta} = \left(R_D^2 + R_C^2 - 2P_2^0\cos(\theta)R_C R_D\right)f + R_D^2 f_{ADD} \qquad (1)$$

The constants R_D and R_C reflect the strength of the dipolar and CSA interactions respectively (Section S5, ESI†). The sign of the relaxation interference term in $R_C R_D$ alternates depending on both the interaction strength and the angle between the CSA tensor and the dipolar field θ. The terms f and f_{ADD} depend principally on the rotational tumbling time of the molecule, τ_c (Section S5, ESI†). Most notably, as R_c is proportional to the magnitude of the field strength, so too is the difference in relaxation rates:

$$R_2^{I_-S_\alpha} - R_2^{I_-S_\beta} = 4P_2^0\cos(\theta)R_C R_D f. \qquad (2)$$

Rotational tumbling also affects the difference in relaxation rates, through the factor f (Section S5, ESI†).

To verify this dependence, the relaxation rates of a range of synthetic porphyrins (full structures in Fig. S1, ESI†) were analysed: monomer, **P1** (R = *t*-Bu), linear (***l***-) dimer ***l*-P2**

(R = *t*-Bu) and hexamer ***l*-P6** (R = THS), and cyclic (***c***-) hexamers with and without a central template ***c*-P6·T6** (R = THS) and ***c*-P6** (with R = THS and R = OC_8H_{17}). The β-pyrrole proton relaxation rates were measured at four magnetic field strengths whose ^{1}H Larmor frequencies varied from 300 to 950 MHz, yielding four relaxation rates per field per molecule (Fig. 3 and Fig. S4A, ESI†). For each molecule, all data were fitted to eqn (1) with the correlation time, the CSA for spins I and S and the angle between the dipolar and CSA interactions obtained as parameters (Fig. 3, solid lines, and parameters Fig. 4A and D). To verify that the fitting parameters are reliable, we sought to validate them against independent measurements. The experimentally determined correlation time (Fig. 4A) was found to scale with molecular weight (Fig. 4B). An independent measure was obtained from the translational diffusion coefficient[21,22] (D_T) obtained using a pulsed field gradient NMR experiment[23] and the following:

$$\tau_C^{Diff} = \lambda k_B{}^2 T^2 / 162\pi^2 \eta^2 D_T{}^3 \quad (3)$$

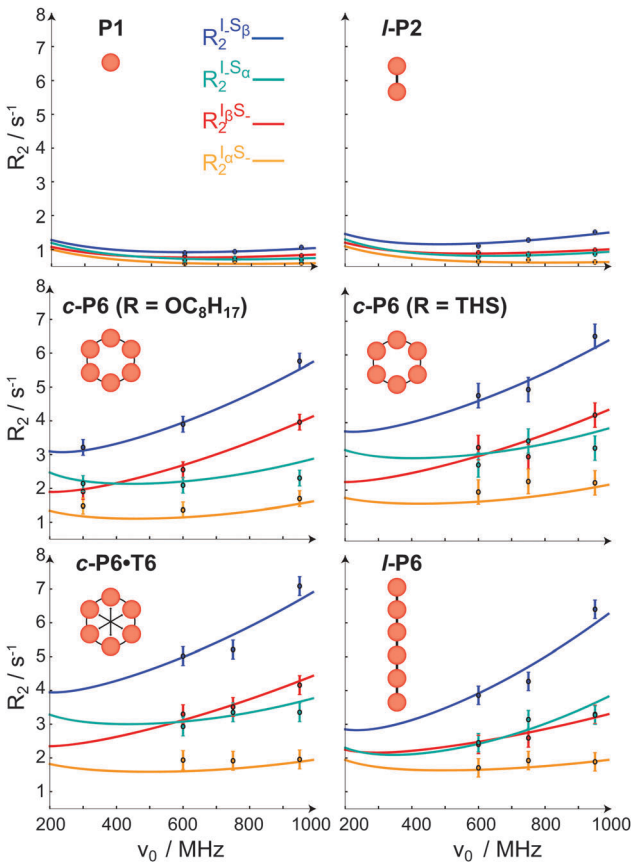

Fig. 3 Plots of relaxation rates (R_2) as a function of magnetic field strength for I_-S_α, I_-S_β, $I_\alpha S_-$ and $I_\beta S_-$ coherences for each of the six molecules. The points are fit using eqn (1) with CSAs of the two spins, a single correlation time and the angle, θ, used as fitting parameters. Relaxation rates and the difference between multiplet components increase with field strength revealing the effects of the CSA mechanism (eqn (2)). Both the relaxation rates and the differences between multiplet components increase for larger molecules (Fig. S4, ESI†). Error bars reflect a combination of both repeated measurements and fitting errors.

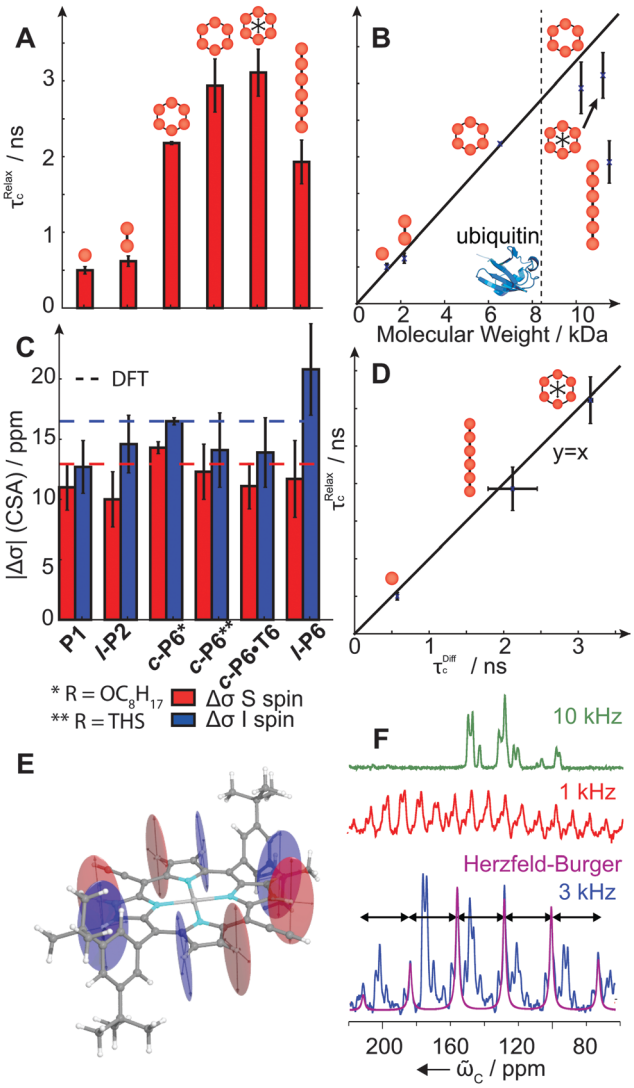

Fig. 4 (A and B) The fitted correlation times for each molecule scale with molecular weight. The linear porphyrin hexamer ***l*-P6** tumbles more rapidly than the cyclic hexamer, as expected. For comparison, the molecular weight of the protein ubiquitin is indicated. (C) Fitted CSAs for I and S spins from the relaxation measurements for each of the molecules, compared to the DFT calculated values. (D) The rotational correlation time can be estimated using translational diffusion measurements. The two correlation times are in close agreement confirming ***l*-P6** tumbles like a rod, not a sphere. (E) Ellipsoid representations of calculated shielding tensors from DFT for I (blue) and S (red) spins in monomer **P1**. The most deshielded component is perpendicular to the plane of the porphyrin for both spins. (F) Solid-state ^{13}C spectra of **P1** at three rotational frequencies. The distribution of rotational side bands at 3 kHz (blue) enabled a Herzfeld–Burger analysis (purple) and determination of the ^{13}C CSA.

where η is the viscosity of the solution and λ is a factor that accounts for non-spherical geometries (Section S7, ESI†). The correlation times from relaxation interference and translational diffusion were in excellent quantitative agreement (Fig. 4D). The experimentally derived CSA values were remarkably constant (Fig. 4C), consistent with the electronic structure of the porphyrin being largely independent of concatenation. To validate this result, we calculated the chemical shielding tensor (Fig. 4E)

using density functional theory (DFT). Specifically, we performed a GIAO B3LYP/6-31G(d) calculation on a B3LYP/6-31(d) optimised structure[24] using Gaussian09.[25] The isotropic chemical shifts were found to be in excellent agreement with those measured experimentally, and in a wide range of benchmark small molecules (Fig. S6A, ESI†).[24,26] Moreover, the chemical shift anisotropy values obtained from calculation also compare favourably with the values from our relaxation experiment (Fig. 4D). Finally, spectral resolution in the ^{13}C spectrum allowed a ^{13}C CSA measurement directly on **P1** using solid-state NMR *via* a Herzfeld-Berger analysis[27] of the spinning side bands (Fig. 4F). These experimental values were consistent with DFT derived values (Table S2, ESI†).

It is interesting to consider why relaxation interference effects are not observed more widely in solution-state NMR spectra. Eqn (1) predicts that differences in intrinsic relaxation should lead to observably different linewidths, even for small molecules.[18] Measurements on **P1**, a single porphyrin, reveal readily distinguishable relaxation rates using our experiment (Fig. S4A, ESI†), yet the 1D NMR spectra can appear largely unchanged. The effect is obscured for low molecular weight complexes as the line width is dominated by magnetic field heterogeneity in the instrument, not the intrinsic linewidth of the molecule, revealed by our measurements. As the molecular weight increases, the line broadening due to slow tumbling makes the effect more prominent. Conversely, since the magnitude of the intensity difference is related to the effective local motional correlation time (Fig. S7, ESI†), any factor that effectively decreases this value by, for example, increasing the temperature, lowering solvent viscosity or the enhanced local internal motion will reduce the appearance of these effect in NMR spectra. As resonances with a higher CSA will have a more pronounced difference in intensities in a scalar coupling pattern, this effect is potentially of use for assignment, as well as for characterisation of supramolecular assemblies.

These results reveal that relaxation interference between dipolar and CSA fields can give rise to apparently anomalous intensities in the scalar coupling patterns of supramolecular complexes. Our experiment and analysis protocols provide a straightforward means to both identify the effect, and measure the tumbling rate and the CSA. As chemists synthesise increasingly complex molecules of ever increasing molecular weight, it will become increasingly helpful to recognise and exploit these effects in their NMR spectra.

We thank the EPSRC (GK, AC), the BBSRC (grant BB/J014346/1, AJB) and the ERC (grant 320969, HLA) for financial support.

Notes and references

1 D. V. Kondratuk, L. M. A. Perdigão, A. M. S. Esmail, J. N. O'Shea, P. H. Beton and H. L. Anderson, *Nat. Chem.*, 2015, **7**, 317–322.
2 M. Hoffmann, J. Kärnbratt, M. H. Chang, L. M. Herz, B. Albinsson and H. L. Anderson, *Angew. Chem., Int. Ed.*, 2008, **47**, 4993–4996.
3 J. K. Sprafke, D. V. Kondratuk, M. Wykes, A. L. Thompson, M. Hoffmann, R. Drevinskas, W. H. Chen, C. K. Yong, J. Kärnbratt, J. E. Bullock, M. Malfois, M. R. Wasielewski, B. Albinsson, L. M. Herz, D. Zigmantas, D. Beljonne and H. L. Anderson, *J. Am. Chem. Soc.*, 2011, **133**, 17262–17273.
4 M. Hutin, J. K. Sprafke, B. Odell, H. L. Anderson and T. D. W. Claridge, *J. Am. Chem. Soc.*, 2013, **135**, 12798–12807.
5 P. Neuhaus, A. Cnossen, J. Q. Gong, L. M. Herz and H. L. Anderson, *Angew. Chem., Int. Ed.*, 2015, **54**, 7344–7348.
6 N. Bloembergen, E. Purcell and R. Pound, *Phys. Rev.*, 1948, **73**, 679–715.
7 A. G. Redfield, *IBM J. Res. Dev.*, 1957, **1**, 19–31.
8 M. Goldman, *J. Magn. Reson.*, 1984, **60**, 437–452.
9 I. Kuprov and P. J. Hore, *J. Magn. Reson.*, 2004, **168**, 1–7.
10 K. Pervushin, R. Riek, G. Wider and K. Wuthrich, *Proc. Natl. Acad. Sci. U. S. A.*, 1997, **94**, 12366–12371.
11 J. E. Ollerenshaw, V. Tugarinov and L. E. Kay, *Magn. Reson. Chem.*, 2003, **41**, 843–852.
12 V. Tugarinov, P. M. Hwang, J. E. Ollerenshaw and L. E. Kay, *J. Am. Chem. Soc.*, 2003, **125**, 10420–10428.
13 A. J. Baldwin and L. E. Kay, *Nat. Chem. Biol.*, 2009, **5**, 808–814.
14 A. J. Baldwin, D. F. Hansen, P. Vallurupalli and L. E. Kay, *J. Am. Chem. Soc.*, 2009, **131**, 11939–11948.
15 H. Carr and E. Purcell, *Phys. Rev.*, 1954, **94**, 630–638.
16 S. Meiboom and D. Gill, *Rev. Sci. Instrum.*, 1958, **29**, 688.
17 J. A. Aguilar, M. Nilsson, G. Bodenhausen and G. A. Morris, *Chem. Commun.*, 2012, **48**, 811–813.
18 R. L. Vold and R. R. Vold, *Prog. Nucl. Magn. Reson. Spectrosc.*, 1978, **12**, 79–133.
19 L. Emsley, J. Kowalewski and G. Bodenhausen, *Appl. Magn. Reson.*, 1990, **1**, 139–147.
20 J. Cavanagh, W. J. Fairbrother, A. G. Palmer III, M. Rance and N. J. Skelton, *Protein NMR Spectroscopy: Principles and Practice*, Academic Press, 2007.
21 S. Yao, J. J. Babon and R. S. Norton, *Biophys. Chem.*, 2008, **136**, 145–151.
22 A. J. Baldwin, J. Christodoulou, P. D. Barker, C. M. Dobson and G. Lippens, *J. Chem. Phys.*, 2007, **127**, 114505.
23 A. Jerschow and N. Müller, *J. Magn. Reson.*, 1997, **125**, 372–375.
24 M. W. Lodewyk, M. R. Siebert and D. J. Tantillo, *Chem. Rev.*, 2012, **112**, 1839–1862.
25 M. J. Frisch, *et al.*, *Gaussian 09, Revision D.01*, Gaussian Inc., Wallingford CT, 2009.
26 SDBS. Web: http://sdbs.db.aist.go.jp. National Institute of Advanced Industrial Science and Technology (Japan), accessed May, 2015.
27 J. Herzfeld and A. E. Berger, *J. Chem. Phys.*, 1980, **73**, 6021.

